https://doi.org/10.15407/ujpe65.12.1109

V. BORYSIUK

Sumy State University
*(2, Rimskii-Korsakov Str., Sumy 40007, Ukraine; e-mail: v.borisyuk@phe.sumdu.edu.ua)*

# MECHANICAL PROPERTIES OF $Ti_{n+1}AlC_n$ NANOLAMINATES: A MOLECULAR DYNAMICS STUDY

*The behavior of $Ti_{n+1}AlC_n$ nanolaminates with $n = 1$, 2, 3 that undergo a tensile deformation has been simulated using classical molecular dynamics methods. While calculating interatomic forces, a combination of two- and three-body potentials together with the embedded-atom method is applied. The stress-strain curves and the approximate values of the elastic moduli for the researched samples are calculated. The strain rate effect on the fracture dynamics is considered, and the corresponding atomistic configurations of examined samples are built.*

*K e y w o r d s*: molecular dynamics, deformation, elastic modulus, strain rate.

## 1. Introduction

Ternary compounds $Ti_{n+1}AlC_n$ are representatives of a relatively new class of solids, the so-called MAX phases, where M denotes a transition metal, A is one of the elements of group A in the table of chemical elements, and X stands for carbon or nitrogen [1]. Those materials have unique physical, chemical, and mechanical properties, being highly promising for applications [1, 2]. In particular, under various conditions, $Ti_{n+1}AlC_n$ nanolaminates combine the characteristics of metals and ceramics. They are characterized by high electrical and thermal conductivities, a relatively high value of the elastic modulus, and an increased resistance to corrosion and oxidation [2]. $Ti_{n+1}AlC_n$ nanolaminates have a layered structure, in which the layers of aluminium atoms and the layers of titanium carbide $Ti_{n+1}C_n$ alternate, as is shown in Fig. 1. A unit cell of their crystal lattice belongs to the hexagonal type [2].

The simulation of multicomponent compounds with chemical bonds of different types using the molecular dynamics method is a rather difficult task, because, as a rule, it requires the application of special interatomic interaction potentials for simulating the corresponding chemical bonds, which should provide an equilibrium configuration of atoms in the final substance. Hence, before studying the mechanical properties of ternary nanostructured compounds $Ti_{n+1}AlC_n$ in the framework of the classical molecular dynamics, an appropriate model for calculating the interatomic interaction forces should be chosen. This model has to provide a representation of the structure of an examined material close to the real one.

Recent researches [5, 6] have shown that MAX phases are characterized by a combination of metallic, covalent, and ionic chemical bonds. Therefore, one of the possible variants consists in the application of several different potentials of interatomic interaction to simulate the bonds between the atoms of different types. To simulate the interaction between the titanium and aluminium atoms, the embedded-atom method (EAM) [7] was used. The analytical expressions for equations describing the energy of interaction between titanium and aluminium atoms in the EAM model and the corresponding numerical parameters can be found in works [7, 8].

The interaction forces between the titanium and carbon atoms were calculated using the model that was applied in works [9–11]. A detailed description

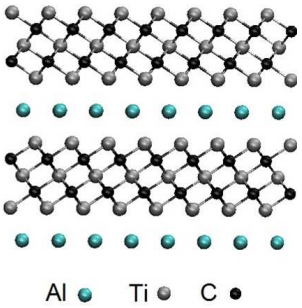


***Fig. 1.*** Atomistic structure of $Ti_3AlC_2$ nanolaminate

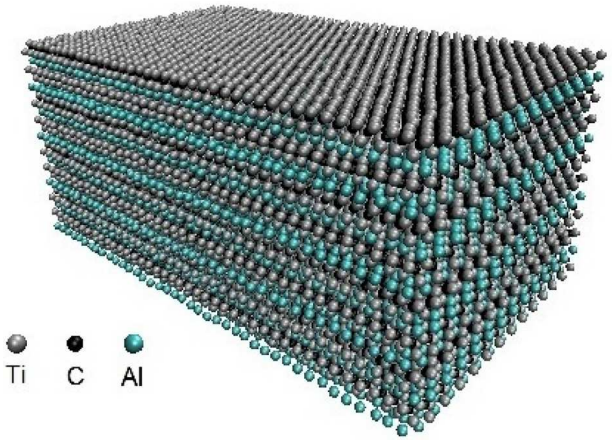


***Fig. 2.*** Initial atomistic configuration of the $Ti_2AlC$ sample

of this approach for simulating the titanium-carbon interaction can be found in works [9, 12], with only a brief summary of the model being given below.

According to this scheme, the potential energy of the system can be represented as the sum of a two- and a three-particle term [12]. The potential energy of pair interaction was described by the Lennard-Jones potential in the standard form [13]

$$U_{ij} = \varepsilon_0 \left[ \left( \frac{r_0}{r_{ij}} \right)^{12} - 2 \left( \frac{r_0}{r_{ij}} \right)^{6} \right], \tag{1}$$

where $r_{ij}$ is the distance between the $i$-th and $j$-th atoms, $r_0$ the corresponding equilibrium distance, and $\varepsilon_0$ the value of the interatomic interaction energy at its minimum. On the other hand, the interaction energy of three atoms $i$, $j$, and $k$ is determined by the Axilrod–Teller potential [14]

$$W_{ijk} = \frac{Z(1 + \cos\theta_i \cos\theta_j \cos\theta_k)}{(r_{ij} r_{ik} r_{jk})^3}, \tag{2}$$

where $r_{ij}$, $r_{ik}$, and $r_{jk}$ are the distances between the atomic pairs $i-j$, $i-k$, and $j-k$, respectively; $Z$ is the intensity parameter of the three-particle interaction; and $\theta_i$, $\theta_j$, and $\theta_k$ are the angles in the triangle formed by the vectors $\mathbf{r}_{ij}$, $\mathbf{r}_{ik}$, and $\mathbf{r}_{jk}$. The numerical values of the parameters for the Lennard-Jones and Axilrod–Teller potentials in the case of C–Ti interaction were calculated in work [12], while modeling the interaction of titanium atoms with carbon nanotubes. The interaction between carbon atoms themselves was simulated by the Lennard-Jones potential, as was done in work [15].

In such a way, a numerical model was obtained for atomistic simulation of the behavior of $Ti_{n+1}AlC_n$ compounds in the framework of the molecular dynamics methods. In this work, we will study the fracture dynamics of three $Ti_{n+1}AlC_n$ nanomaterials with $n = 1, 2, 3$ and will calculate the approximate values for their mechanical parameters.

## 2. Computer Model of Specimens and the Deformation Procedure

Before starting the simulation, titanium, aluminium, and carbon atoms were arranged at the sites of a perfect crystal lattice corresponding to the crystalline structure of $Ti_{n+1}AlC_n$. Then, the specimens were relaxed to the equilibrium at a temperature of 300 K maintained by means of a Berendsen thermostat [16]. The general view of model specimens is shown in Fig. 2 by an example of the $Ti_2AlC$ structure.

When studying the mechanical properties of $Ti_{n+1}AlC_n$, a numerical tensile deformation procedure was also used to calculate the dependence of the mechanical stress $\sigma$ on the strain $\varepsilon$. The external action was simulated as follows. The atoms located in five rightmost atomic layers of the sample were displaced at a constant rate, whereas five leftmost atomic layers remained fixed. The direction of the applied displacement was chosen so that the distance between the opposite sample ends was gradually increasing as the sample was being stretched. In addition, in order to study the influence of the strain rate $d\varepsilon/dt$ on the fracture dynamics, the specimens were stretched at three different values of this parameter.

In the course of a sample deformation, mechanical stresses were calculated on the basis of the virtual

theorem using the formula [17–19]

$$\sigma_{ij} = \frac{1}{V}\sum_{\alpha=1}^{N}\left(\frac{1}{2}\sum_{\beta=1}^{N} r^i_{\alpha\beta} f^j_{\alpha\beta} - m^\alpha v^\alpha_i v^\alpha_j\right), \qquad (3)$$

where the indices $i$ and $j$ mark the components in the Cartesian coordinates; the indices $\alpha$ and $\beta$ enumerate the atoms; $r^i_{\alpha\beta}$ and $f^j_{\alpha\beta}$ are the corresponding components of the distance and force, respectively, vectors between the atoms $\alpha$ and $\beta$; $m$ is the atomic mass; $N$ the number of atoms in the sample; and $V$ the sample volume. Thus, by calculating the corresponding components of the velocities and the forces of interatomic interaction at a given strain $\varepsilon$, we can obtain the stress-strain curve $\sigma(\varepsilon)$.

## 3. Simulation Results. Calculation of Mechanical Parameters

The calculation results obtained by formula (3) for the dependences of the mechanical stress $\sigma$ on the strain $\varepsilon$ for the $Ti_2AlC$ sample at various strain rates are depicted in Fig. 3. One can see that all stress-strain curves have a typical profile. The initial sections of the dependences correspond to elastic deformations. The further growth and, afterward, the recession of the dependences characterize the plastic deformation and the failure of the samples. It should also be noted that the curves obtained for the $Ti_2AlC$ sample in the case where the strain rate $d\varepsilon/dt$ grows demonstrate a small increase of the strain and stress critical values ($\varepsilon_c$ and $\sigma_c$, respectively) at which the sample failure begins.

The corresponding "elastic" sections in the dependences $\sigma(\varepsilon)$ at small strains $\varepsilon \leq 0.005$ are shown in Fig. 4. Note that, in order to calculate the elastic modulus, the procedure of linear approximation of the obtained numerical data by the least squares method has to be applied. In doing so, one should bear in mind that the available fluctuations in the calculated stress-strain curves make the values obtained for the elastic modulus in such a way to be strongly dependent on the $\varepsilon$-interval of the $\sigma(\varepsilon)$ curve that was selected for the approximation. The values presented below for the elastic modulus $Y$ were calculated in the interval $\varepsilon \leq 0.002$ with an accuracy of 10 GPa. In particular, for $Ti_2AlC$, the value $Y_{Ti_2AlC} \approx 280$ GPa was obtained. This value agrees well with the data available in the literature [5, 20, 21]. For instance, in

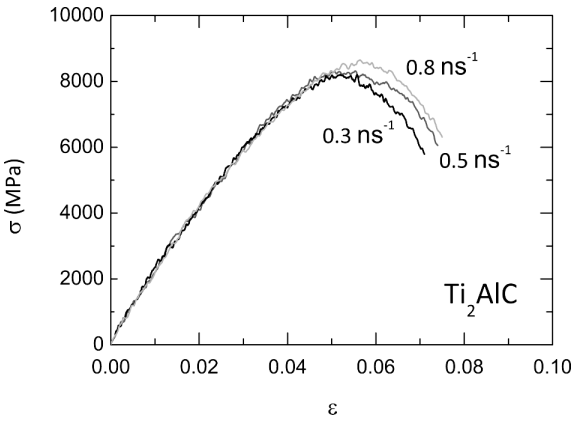


***Fig. 3.*** Stress-strain curves for the $Ti_2AlC$ sample calculated at various strain rates (indicated in the figure)

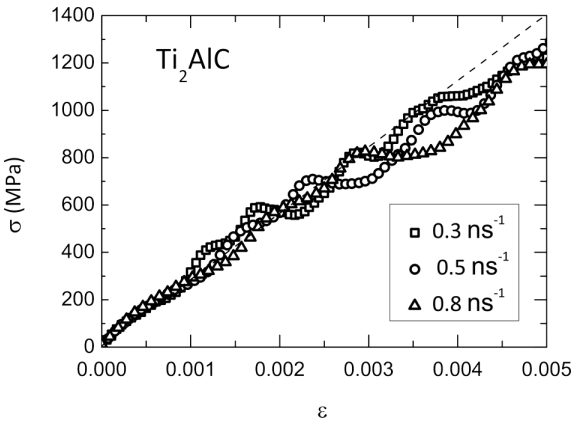


***Fig. 4.*** Elastic sections of the stress-strain curves for the $Ti_2AlC$ sample at various strain rates. The dashed line corresponds to an elastic modulus of 280 GPa

work [20], the experimentally measured value of the elastic modulus for $Ti_2AlC$ was equal to $Y_{Ti_2AlC} \approx 278$ GPa. On the other hand, the *ab initio* calculations gave rise to a value of 312 GPa [5].

Atomistic configurations of the $Ti_2AlC$ sample at various strains are shown in Fig. 5. One can see that the sample undergoes a substantial failure at the strains $\varepsilon > 0.05$. It should be noted that the failure of the $Ti_2AlC$ sample was not accompanied by the formation of connective "bottlenecks", which are characteristic of the metal failure.

The $Ti_3AlC_2$ and $Ti_4AlC_3$ samples were studied following the same procedure. The corresponding stress-strain curves calculated for them at various strain rates are shown in Fig. 6 [panels ($a$) and ($b$), re-

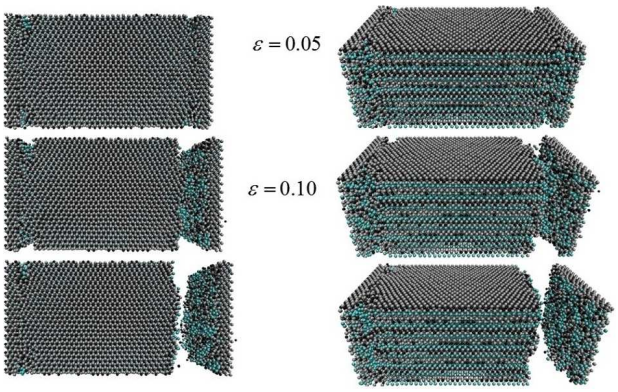


***Fig. 5.*** Atomistic configurations of the $Ti_2AlC$ sample at various strains $\varepsilon$'s: top view (left panels) and side view (right panels). The strain values are indicated. The lower panels illustrate the sample after its failure

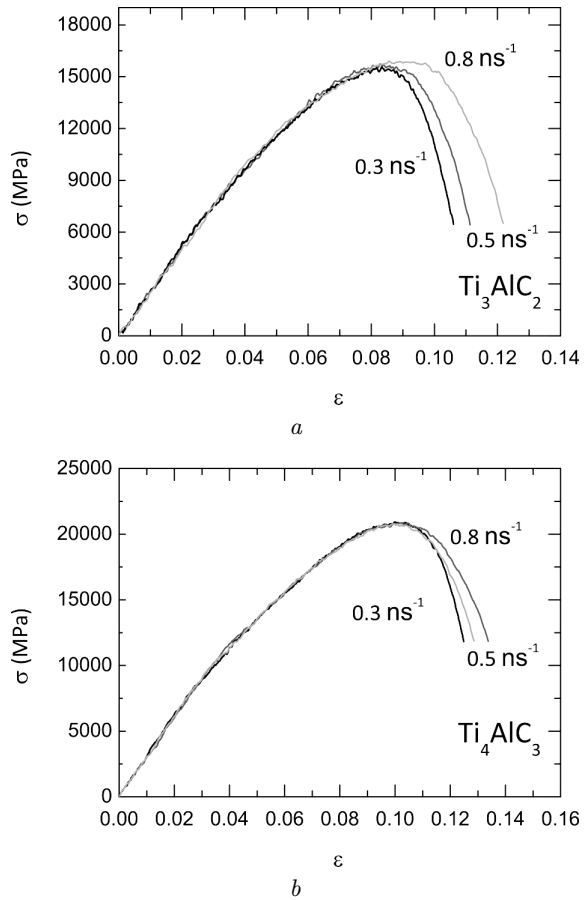


***Fig. 6.*** Stress-strain curves for the $Ti_3AlC_2$ ($a$) and $Ti_4AlC_3$ ($b$) samples calculated at various strain rates (indicated in the figure)

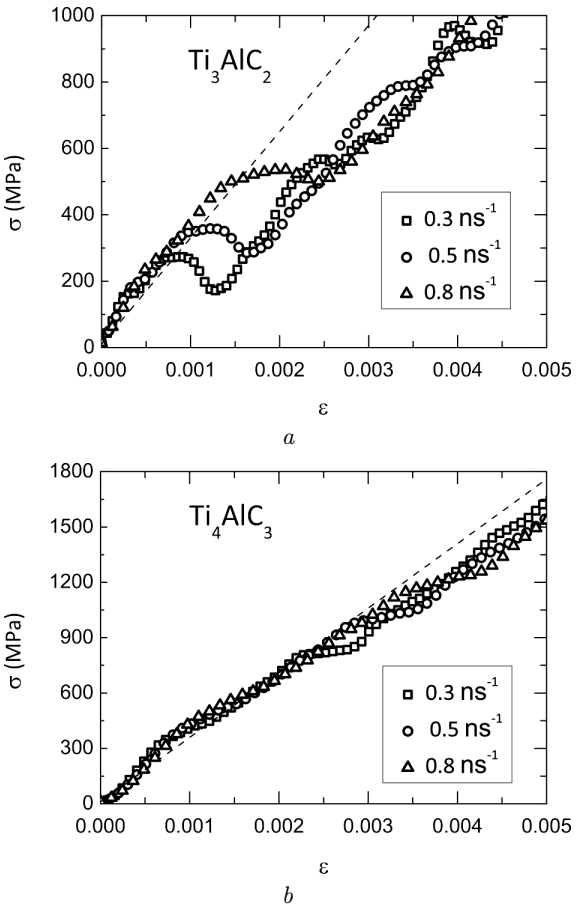


***Fig. 7.*** Elastic sections of the stress-strain curves for the $Ti_3AlC_2$ ($a$) and $Ti_4AlC_3$ ($b$) samples at various strain rates (indicated in the figure). The dashed lines correspond to elastic moduli of 320 GPa (panel $a$) and 350 GPa (panel $b$)

spectively]. The obtained dependences have a typical form with the sections corresponding to elastic and plastic deformations. They are also characterized by the dependence of the critical strain $\varepsilon_c$ on the strain rate $d\varepsilon/dt$.

The corresponding "elastic" sections of the stress-strain curves at small strains $\varepsilon \leq 0.005$ are exhibited in Fig. 7. The presented dependences testify that the $Ti_4AlC_3$ sample is characterized by a larger approximated value of the elastic modulus ($Y_{Ti_4AlC_3} \approx 350$ GPa) than the $Ti_3AlC_2$ sample ($Y_{Ti_3AlC_2} \approx 320$ GPa), which is in qualitative agreement with the literature data (403 and 368 GPa, respectively) obtained from the first principles [5]. Furthermore, there is an experimentally measured value

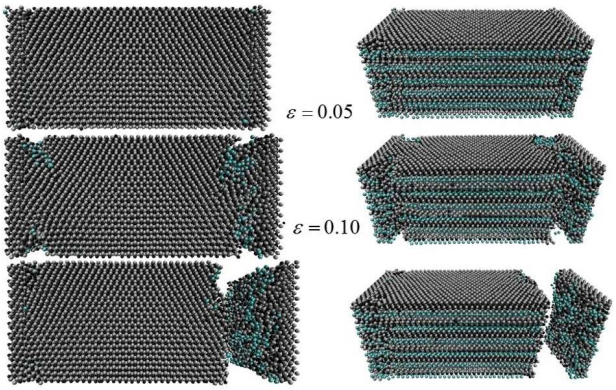


***Fig. 8.*** Atomistic configurations of the $Ti_3AlC_2$ sample at various strains $\varepsilon$'s: top view (left panels) and side view (right panels). The strain values are indicated. The lower panels illustrate the sample after its failure

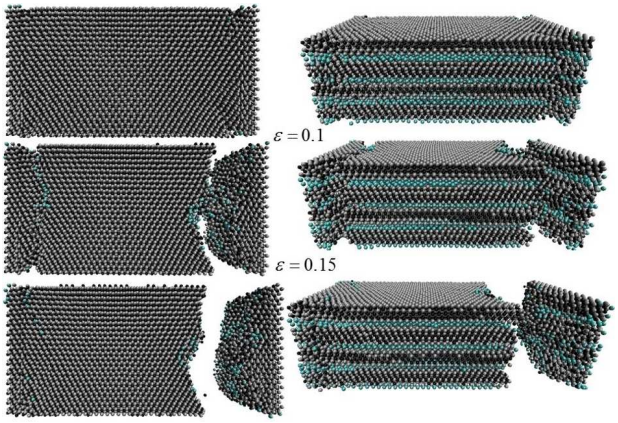


***Fig. 9.*** Atomistic configurations of the $Ti_4AlC_3$ sample at various strains $\varepsilon$'s: top view (left panels) and side view (right panels). The strain values are indicated. The lower panels illustrate the sample after its failure

of 298 GPa for the $Ti_3AlC_2$ sample in [21], which is also consistent with the value obtained in this work.

Atomistic configurations of the researched $Ti_3AlC_2$ and $Ti_4AlC_3$ samples at various strains are shown in Figs. 8 and 9, respectively. As one can see, the failure of those samples is accompanied by a more intense formation of connecting "bottlenecks" at the sample right side that moves at a constant rate. Cracks also appear in the same way at the opposite sample side, which contains atoms that are fixed in space. The cracks formed during the deformation process disappear after the sample failure, and there appear residual deformations localized in this area.

The results of calculations show that the growth of the parameter $n$ in the chemical formula $Ti_{n+1}AlC_n$ gives rise to larger values of the elastic modulus for the corresponding samples. In addition, the $Ti_{n+1}AlC_n$ samples with different $n$'s are characterized by different critical strain values $\varepsilon_c$ corresponding to the beginning of the sample failure. In order to compare the critical strain values of all examined samples, the corresponding stress-strain curves $\sigma(\varepsilon)$ calculated for the strain rate $d\varepsilon/dt = 0.5$ ns$^{-1}$ are shown in Fig. 10. One can see that the $Ti_2AlC$ sample with the lowest elastic modulus has the lowest critical strain value $\varepsilon_c^{Ti_2AlC} \approx 0.055$. For the $Ti_3AlC_2$ and $Ti_4AlC_3$ samples, the $\varepsilon_c$-values are $\varepsilon_c^{Ti_3AlC_2} \approx 0.085$ and $\varepsilon_c^{Ti_4AlC_3} \approx 0.105$. This behavior is obviously associated with different relative numbers of Ti–C and Ti–Al chemical bonds distributed over the sample volume, which are characterized by different values of the equilibrium interatomic distance and the interaction strength.

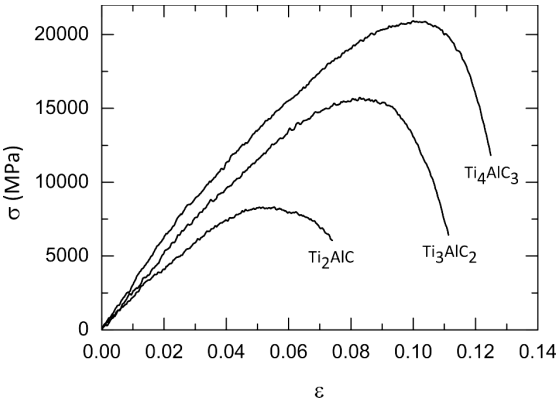


***Fig. 10.*** Stress-strain curves for the $Ti_{n+1}AlC_n$ samples with $n = 1, 2, 3$ at the strain rate $d\varepsilon/dt = 0.5$ ns$^{-1}$

## 4. Conclusions

Mechanical properties of three-component nanolaminates $Ti_{n+1}AlC_n$ with $n = 1, 2, 3$ have been analyzed. The dynamics of the sample failure under the action of a tensile deformation is considered. For all three samples, the corresponding stress-strain curves at various strain rates are calculated, and the approximate values of the elastic modulus are determined: $Y \approx 280$ GPa for $Ti_{n+1}AlC_n$, $Y \approx 320$ GPa for $Ti_3AlC_2$, and $Y \approx 350$ GPa for $Ti_4AlC_3$. The obtained stress-strain curves testify that, for the major-

ity of researched materials, the growth of the strain rate $d\varepsilon/dt$ leads to a small increase of the critical strain value $\varepsilon_c$ at which the sample begins to break.

*The research was carried out in the framework of the grant of the President of Ukraine (project No. 0116U006576 of the State Fund for Fundamental Research). The author is also grateful for the financial support of the Ministry of Education and Science of Ukraine (project No. 0117U003923).*

1. M.W. Barsoum. The $M_{N+1}AX_N$ phases: a new class of solids: thermodynamically stable nanolaminates. *Progr. Solid State Chem.* **28**, 201 (2000).
2. M.W. Barsoum. *MAX Phases: Properties of Machinable Ternary Carbides and Nitrides* (Wiley, 2013) [ISBN: 978-3-527-65460-4].
3. Q. Tang, Z. Zhou, P.W. Shen. Are MXenes promising anode materials for Li ion batteries? Computational studies on electronic properties and Li storage capability of $Ti_3C_2$ and $Ti_3C_2X_2$ (X = F, OH) monolayer. *J. Am. Chem. Soc.* **134**, 16909 (2012).
4. Y. Xie, P.R.C. Kent. Hybrid density functional study of structural and electronic properties of functionalized $Ti_{n+1}X_n$ (X=C, N) monolayers. *Phys. Rev. B* **87**, 235441 (2013).
5. M. Naguib, V.N. Mochalin, M.W. Barsoum, Y. Gogotsi. 25th anniversary article: MXenes: A new family of two-dimensional materials. *Adv. Mater.* **26**, 992 (2014).
6. M. Naguib, M. Kurtoglu, V. Presser, J. Lu, J. Niu, M. Heon, L. Hultman, Y. Gogotsi, M.W. Barsoum. Two-dimensional nanocrystals produced by exfoliation of $Ti_3AlC_2$. *Adv. Mater.* **23**, 4248 (2011).
7. X.W. Zhou, H.N.G. Wadley, R.A. Johnson, D.J. Larson, N. Tabat A. Cerezo, A.K. Petford-Long, G.D.W. Smith, P.H. Clifton, R.L. Martens, T.F. Kelly. Atomic scale structure of sputtered metal multilayers. *Acta Materialia* **49**, 4005 (2001).
8. W. Zou, H.N.G. Wadley, X.W. Zhou, S. Ghosal, R. Kosut, D. Brownell. Growth of giant magnetoresistance multilayers: Effects of processing conditions during radio-frequency diode deposition. *J. Vac. Sci. Technol. A* **19**, 2414 (2001).
9. V.N. Borysiuk, V.N. Mochalin, Y. Gogotsi. Molecular dynamic study of the mechanical properties of two-dimensional titanium carbides $Ti_{(n+1)}C_{(n)}$ (MXenes). *Nanotechnology* **26**, 265705 (2015).
10. V.N. Borysiuk, V.N. Mochalin. Thermal stability of two-dimensional titanium carbides $Ti_{(n+1)}C_{(n)}$ (MXenes) from classical molecular dynamics simulations. *MRS Commun.* **9**, 203 (2019).
11. V.N. Borysiuk, V.N. Mochalin, Y. Gogotsi. Bending rigidity of two-dimensional titanium carbide (MXene) nanoribbons: A molecular dynamics study. *Comput. Mater. Sci.* **143**, 418 (2018).
12. H. Oymak, F. Erkoc. Titanium coverage on a single-wall carbon nanotube: molecular dynamics simulations. *Chem. Phys.* **300**, 277 (2004).
13. J.E. Jones. On the determination of molecular fields. II. From the equation of state of a gas. *Proc. R. Soc. Lond. A.* **106**, 463 (1924).
14. B.M. Axilrod, E. Teller. Interaction of the van der Waals type between three atoms. *J. Chem. Phys.* **11**, 299 (1943).
15. N. Sasaki, K. Kobayashi, M. Tsukada. Atomic-scale friction image of graphite in atomic-force microscopy. *Phys. Rev. B* **143**, 2138 (1996).
16. H.J.C. Berendsen, J.P.M. Postma, W.F. van Gunsteren, A. DiNola, J.R. Haak. Molecular-dynamics with coupling to an external bath. *J. Chem. Phys.* **81**, 3684 (1984).
17. D.H. Tsai. The virial theorem and stress calculation in molecular dynamics. *J. Chem. Phys.* **70**, 1375 (1979).
18. A.Hadizadeh Kheirkhah, E.Saeivar Iranizad, M.Raeisi, A.Rajabpour. Mechanical properties of hydrogen functionalized graphene under shear deformation: A molecular dynamics study. *Solid State Commun.* **177**, 98 (2014).
19. V. Borysiuk, I. Lyashenko. Modeling of the elastic properties of the core-shell Au-Ag nanorod. In *Proceedings of the IEEE 36th International Conference on Electronics and Nanotechnology (ELNANO-2016)* (Springer, Wiley, 2016), p. 118.
20. A.G. Zhou, M.W. Barsoum, S. Basu, S.R. Kalidindi, T. El-Raghy. Incipient and regular kink bands in fully dense and 10 vol.% porous $Ti_2AlC$. *Acta Materialia* **54**, 1631 (2006).
21. A.G. Zhou, M.W. Barsoum. Kinking nonlinear elastic deformation of $Ti_3AlC_2$, $Ti_2AlC$, $Ti_3Al(C_{0.5}, N_{0.5})_2$ and $Ti_2Al(C_{0.5}, N_{0.5})$. *J. Alloy. Compd.* **498**, 62 (2010).

Received 22.01.20.
Translated from Ukrainian by O.I. Voitenko

*В.М. Борисюк*

МЕХАНІЧНІ ВЛАСТИВОСТІ НАНОЛАМІНАТІВ $Ti_{n+1}AlC_n$: ДОСЛІДЖЕННЯ МЕТОДАМИ МОЛЕКУЛЯРНОЇ ДИНАМІКИ

Р е з ю м е

Проведено моделювання поведінки наноламінатів $Ti_{n+1}AlC_n$ з $n = 1, 2, 3$ при деформації розтягнення на основі методів класичної молекулярної динаміки. Для розрахунків сил міжатомної взаємодії в досліджуваних зразках був використаний підхід із комбінацією парного та тричастинкового потенціалів і моделі зануреного атома. Для розглянутих зразків розраховано криві навантаження та наближені значення механічних параметрів, а саме модулів пружності. Досліджено вплив швидкості деформації на динаміку руйнування, а також побудовано відповідні атомістичні конфігурації досліджуваних зразків.